Sized-Fiber Reflectometry for Measuring Local Optical Properties

Theodore P. Moffitt and S. A. Prahl

Abstract—**Sized-fiber spectroscopy describes a device and method for measuring absorption and reduced scattering properties of tissue using optical fibers with different diameters. The device used in this paper consists of two fibers with diameters of 200 and 600 μm. Each fiber emits and collects its own backscattered light. Backscattered light measurements for solutions with absorption coefficients of 0.1–2.0 cm^{-1} and reduced scattering coefficients of 5–50 cm^{-1} demonstrate that the device is most sensitive for the highest scattering materials. Monte Carlo simulations suggest the device is insensitive to the fiber illumination characteristics and that the light returning to the fiber is nearly uniform over all directions. Finally, experiments and Monte Carlo simulations of the sized-fiber device indicate that 50% of the signal arises from roughly 1.2 and 1.9 reduced mean-free paths for the 200- and 600-μm fibers, respectively.**

Index Terms—**Absorption, penetration depth, reflectance, scattering, tissue.**

I. Introduction

DETERMINING the optical scattering and absorption properties of tissue for diagnostic and therapeutic applications is of interest in medicine. For example, the dosimetry of photodynamic therapy is greatly dependent upon the scattering and absorption properties [1], [2] for both light delivery and measurement of drug concentrations. Optical properties have been used to estimate exogenous [3], [4] and endogenous [5] chromophore concentrations. Moreover, light scattering and absorption can provide information about both chromophore content and structure, which might be used to distinguish normal and malignant tissues as well as chemical state information [6], [7] (e.g., oxy- versus deoxy-hemoglobin). In this regard, an optical biopsy can be performed using optical information of hemoglobin and water content differences in normal and malignant tissue [8], [9].

Several techniques and algorithms have been developed to measure the optical properties. Spatially [10]–[12] and temporally [13]–[15] resolved measurements have been proposed to extract the optical properties using light distributions based on diffusion theory [16], [17] and/or Monte Carlo simulations [18]. A wide variety of algorithms have been explored to extract optical properties including neural network [19] and multiple polynomial regression methods [20]. However, most reflectance techniques rely on light distribution information over a large area (> 1 cm^2) or have separate illumination and collection fibers with a separation distance on the order of 1 cm.

Much work has been compiled on devices with separate source and detector fibers. Two studies show that the mean photon penetration depth increases as the square root of the separation between source and detector fibers either spatially [21] or temporally [22]. Source–detector fiber devices sample relatively large volumes, because of the separation between the fibers. Though effort has been made to minimize the sampling volume using small source–detector separations [23], little work has been done on photon penetration depths when the source fiber is also used to collect backscattered photons [24]. Since large sampling volumes are less likely to be homogenous, we developed a device that acquires information from small volumes of tissue (< 1 mm^3) by using the same fiber for both source and detector to minimize the sampling volume.

We propose a compact dual-fiber device to make simple and rapid measurements of the absorption and reduced scattering properties of tissue. Each fiber illuminates and collects light independently of the other fiber. The device is based on the fact that, in general, tissues with different scattering and absorption properties will scatter different numbers of photons back into a fiber. If only a single fiber is used, two samples with different optical properties could backscatter the same number of photons. This paper proposes a device containing a second, different size fiber to make a second measurement. This second fiber collects information from a different effective volume of the sample than the first fiber.

In this study, we present experiments on an Intralipid tissue model and Monte Carlo simulations to elucidate the details of light emission and collection with a single fiber. As a first step, we conduct single wavelength experiments at 632.8 nm with a device using 200- and 600-μm fibers to assess the feasibility of extracting optical properties for these fiber sizes. We have adapted the sized-fiber system for use with white light (500–800 nm) to measure the wavelength dependent absorption and reduced scattering coefficients (herein referred to as μ_a and $\mu_s' = (1 - g)\mu_s$, respectively). Experimental results are presented for an array of Intralipid solutions of known absorption 0.1–2.0 cm^{-1}, and reduced scattering 5.2–52 cm^{-1}. Monte Carlo simulations of a 200- and 600-μm fiber device are presented for comparison. Also presented are experiments and Monte Carlo simulations of the penetration depth of photons collected by two fiber sizes, 200 and 600 μm in diameter. Finally, Monte Carlo simulations are used to determine the effect numerical aperture of a fiber and the influence of mode filling of the fiber on reflectance measurements.

Manuscript received May 21, 2001; revised October 30, 2001. This work was supported by the National Institute of Health under Grant NIH-CI-R24-CA84587-01.

T. P. Moffitt and S. A. Prahl are with the Oregon Health and Sciences University, Portland, OR 97225 USA (e-mail: prahl@ece.ogi.edu).

Publisher Item Identifier S 1077-260X(01)11195-0.

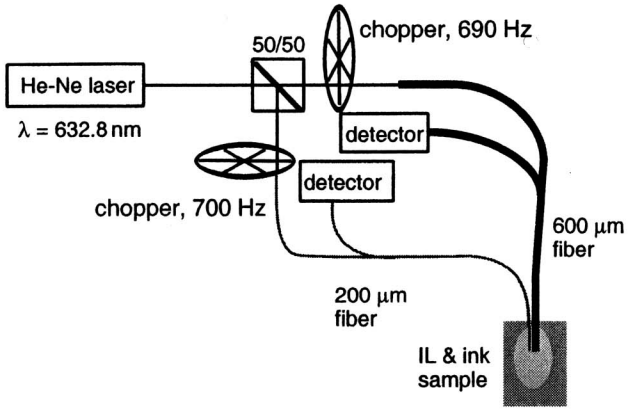

Fig. 1. The sized-fiber device. A pair of bifurcated fibers emit and collect light simultaneously by chopping at two distinct frequencies exceeding 690 Hz. The fibers are submerged at least 1 cm into the Intralipid to eliminate boundary effects.

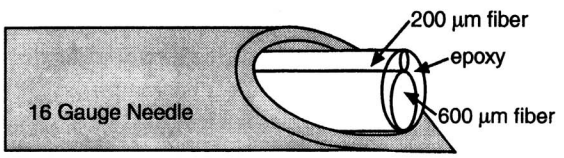

Fig. 2. The 200- and 600-μm fibers are joined with a medical grade epoxy so that they may be simultaneously inserted through a needle for measurement of tissues. The two fibers can easily fit through a 16-gauge needle. When measuring tissues, water is placed at the tip of the fiber to reduce the index mismatch between the fiber cores and the tissue.

II. Materials and Methods

A. Sized-Fiber Device

The sized-fiber device (Fig. 1) uses a pair of bifurcated fibers to separate the illumination light from the backscattered light. The first of these is made by end-coupling two 300-μm-diameter fibers onto the face of a 600-μm-diameter fiber with SMA connectors. The second bifurcated fiber consists of two 100-μm-diameter fibers end-coupled to a 200-μm fiber also using SMA connectors. One of each of the 100- and 300-μm fibers have He–Ne laser light (632.8 nm) focused onto their face. The remaining 100- and 300-μm fibers are coupled to UDT silicon photodiodes. The ends of the 200- and 600-μm fibers are epoxied[1] together by UV curing and then polished (Fig. 2). All fibers are fused silica glass/glass[2] The manufacturer cites a numerical aperture of 0.22, which corresponds to a maximum exit angle of 12.7° in air. We measured $13 \pm 1°$ for both emission and transmission with the 200- and 600-μm fibers for the maximum acceptance angle. The maximum half-angle for acceptance (θ) depends on the numerical aperture of the fiber $\mathrm{NA} = n \sin\theta$, where n is the index of refraction of the surrounding medium. This corresponds to an angle of 9.5° for our fibers in water. The distal ends of the 200- and 600-μm fibers are sleeved through one meter of polycarbonate tubing (6.2-mm O.D., 4.7-mm I.D.) to inhibit tight bending of the fibers. The 100- and 300-μm fibers outside the polycarbonate tubing are kept fixed throughout the experiments so that losses through the fiber cladding remain relatively constant from measurement to measurement in those sections of fiber. Two choppers[3] operating at 690- and 700-Hz eliminate cross-talk between fibers. The reflectance signal from each fiber is detected by a lock-in amplifier.[4] The fibers are rinsed in a water bath and then washed with ethyl alcohol between measurements. Washing the fibers is critical for reproducibility with the Intralipid tissue model which can leave an oily residue on the fiber that affects later measurements.

The sized-fiber device also works with white light reflectometry [25]. A tungsten-halogen white lamp[5] couples to the source fibers via the SMA connectors. The collection fibers are coupled into a spectrometer.[6] The spectrum is processed in near real-time using LabView.[7] A baffle must be inserted so that only one fiber emits and collects at a time, since cross-talk will not be rejected with this method.

All data points are normalized by using Fresnel reflection from the fiber face in air and water. The voltage returned from the photodiode is converted by

$$\text{Reflectance} = \frac{(V_{\text{sample}} - V_{\text{water}})}{(V_{\text{air}} - V_{\text{water}})} * (3.46\% - 0.19\%) + 0.19\%$$

where 3.46% is the Fresnel reflectance for the fiber core/air junction and 0.19% is the Fresnel reflectance for the fiber core/water junction at normal incidence. Measurements of the air and water Fresnel reflectance are taken periodically throughout the experiments to correct for any variations in laser power.

B. Tissue Model

For tissue phantoms with known absorption and reduced scattering properties, an array of Intralipid[8] and India ink mixtures with optical properties in the range of tissues were constructed. Five dilutions of the Intralipid are made from a single bottle of Intralipid making concentrations of 1%, 2%, 4%, 9%, and 10% (10% lipid indicates 10 g of lipid per 100 ml of suspension) to be used as stock solutions. Also, five stock solutions of India ink[9] and deionized/distilled water are made with absorption of 0.2, 0.4, 1.0, 2.0, and 4.0 cm^{-1} at 632 nm as measured using a spectrophotometer (HP 8452A). The absorption of light at 632 nm by Intralipid [26] is less than 0.01 cm^{-1} at the highest concentration, and thus is negligible in comparison to absorption by the India ink. The phantoms are made by mixing one part of each Intralipid concentration to one part of each ink solution for a total of 25 samples. The resultant solutions have all possible combinations of Intralipid concentrations of 0.5%, 1%, 2%, 4.5%, and 5% corresponding to reduced scattering coefficients of 5.2, 10.4, 20.8, 46.8, and 52.0 cm^{-1} and absorption coefficients of 0.1, 0.2, 0.5, 1.0, and 2.0 cm^{-1} at 632 nm. The optical properties are determined by $R(r)$ measurements

[1]120387, Dymax Corporation, Torrington, CT.

[2]Polymicro Technologies LLC, Phoenix, AZ.

[3]MC 1000, Thorlabs Inc., Newton, NJ.

[4]LIA 100, Thorlabs Inc., Newton, NJ.

[5]LS-1, Ocean Optics Inc., Dunedin, FL.

[6]s2000, Ocean Optics Inc., Dunedin, FL.

[7]National Instruments, Austin, TX.

[8]Liposyn II, Abbott Laboratories, North Chicago, IL.

[9]No. 4415, Higgins, Lewisburg, TN.

[16] and cross-checked using total diffuse reflectance measurements using an integrating sphere [27] in conjunction with inverse adding-doubling [28]. We measured a reduced scattering coefficients of 104 cm^{-1}, which is between those of and Flock *et al.* [26] and van Staveren *et al.* [29] who measured of 65 and 130 cm^{-1}, respectively, for 10% Intralipid.

C. Chicken Breast Experiment

Chicken breast was measured using the sized-fiber device inside a 16-gauge needle. The needle was filled with water before inserting the optical fibers to aid the coupling of light between the fibers and the tissue. The needle was inserted into the muscle along the muscle grain in three locations. The needle was withdrawn and inserted so that the needle tip was in the same three locations but oriented perpendicular to the muscle grain for the second set of measurements. All the measurements were performed within 5 min to minimize changes in the optical properties due to dehydration of the tissue. Additionally, paper towels saturated with phosphate-buffered saline covered the chicken between measurements.

D. Planar Absorber Effect on Signal Experiment

To measure the effect of an absorbing boundary on the signal detection, the Thorlabs lock-in amplifiers were replaced by SR830 lock-in amplifiers[10] for their phase-adjustment capability and improved signal-to-noise ratio. Optically thick India ink mixed in acrylamide was used for an absorbing plane. The 1–cm-thick acrylamide was set in the bottom of a 50-ml beaker. The Intralipid phantom described above with an absorption coefficient of 0.5 cm^{-1} and reduced scattering coefficient of 20.8 cm^{-1} covered the black acrylamide layer. The fibers were brought into contact with the gelatin before the Intralipid was added to obtain a zero position. The fibers were backed away from the surface for a distance of 1 cm. Measurements were then recorded for the 200- and 600-μm fiber simultaneously in 0.1-mm increments until the fibers were submerged into the gelatin. At this point, the signal was constant and equal to the Fresnel reflection of the fiber in water. Measurements of the reflectance in air and water were also recorded for calibration.

E. Monte Carlo Simulations

A Monte Carlo program was adapted to simulate the light collected by a fiber irradiating an infinite homogeneous scattering and absorbing medium. The fiber face was the only boundary included in the simulations, thus neglecting the sides of the fiber (e.g., the fiber jacket, etc.). Experimental results confirm the validity of the computer simulations (Fig. 3). Also, the photon penetration depth was tracked to give insight as to the volume being sampled for each size fiber. Additional simulations were performed to examine the effect of photon launching angle and the effect of varying the numerical aperture.

The geometry of the Monte Carlo simulation is set up as follows. Let the z axis be parallel with that of the fiber so that the face of the fiber is in the $z = 0$ plane. Photons are launched with equal probability over the entire face of the fiber. The direction by which photons are launched is specified by the direction

[10]Stanford Research Systems, Sunnyvale, CA.

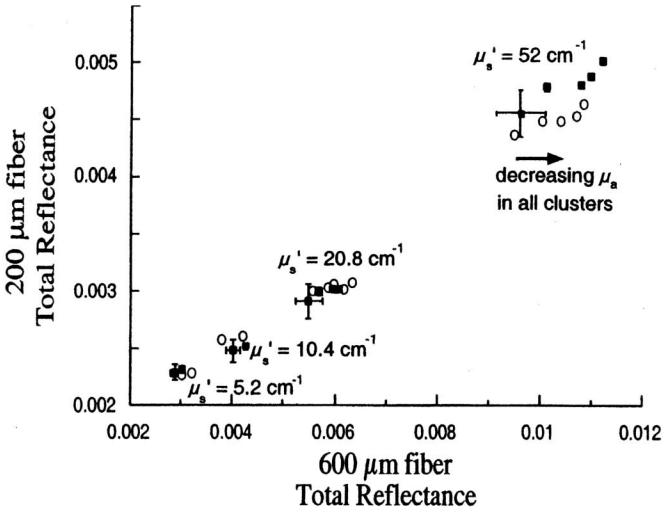

Fig. 3. Optical properties can be determined from a mapping of the reflectance for each fiber. Open circles: experimental measurements of each sample. Solid squares: Monte Carlo simulation results. For samples with $\mu_s' = 5.2$ and 10.4 cm^{-1}, Monte Carlo results are only shown for $\mu_a = 0.1$ and 2.0 cm^{-1} for clarity.

cosines (ν_x, ν_y, ν_z). The angle $\nu_z = \cos\theta_z$ is given a Gaussian distribution that depends on the acceptance angle of the fiber while the other direction cosines are uniformly distributed. The angular distribution chosen approximates the emission from the fibers, but due to under-filled modes, the experimentally measured distribution is not a true Gaussian but only deviates by 12%. The distribution of angles that the photon might take is given by the function

$$p(\theta_z)d\theta_z = \frac{1}{\sqrt{2\pi}} \exp\left(-\frac{\theta_z^2}{2\theta_a^2}\right) d\theta_z$$

where θ_a is the acceptance angle for the fiber. Moreover, the angles were limited such that $\theta_z \leq \theta_a$.

The primary statistic collected by the Monte Carlo program was the fraction of light backscattered into the fiber. Photons which were collected must pass back through the fiber face. Only photons that had an angle less than or equal to the maximum acceptance angle for the fiber were counted into the diffuse reflectance. The maximum acceptance angle for the fiber was input into the program for the fiber in air, then converted using Snell's law for the index of refraction for the incident medium. Photons incident on the fiber face but outside the cone of acceptance were attributed to light lost through the cladding. The acceptance angle was corrected for the index of refraction change of the medium. The index of refraction for the core of the fiber was assumed to be 1.457 as given by the manufacturer's specifications; 1.333 was used for the index of the medium. A returning photon's weight was attenuated due to an index mismatch for both launching and collection using the Fresnel reflection for normal incidence introducing an error $\approx$0.02%. The anisotropy was chosen to be 0.83 in accordance to Flock *et al.* [26]. In a single simulation, a minimum of 20 000 photons were launched ten times for each simulation to accumulate statistical error of the mean. Specular reflectance due to the index mismatch at the fiber face while launching was added to the diffuse reflectance to get the total reflectance.

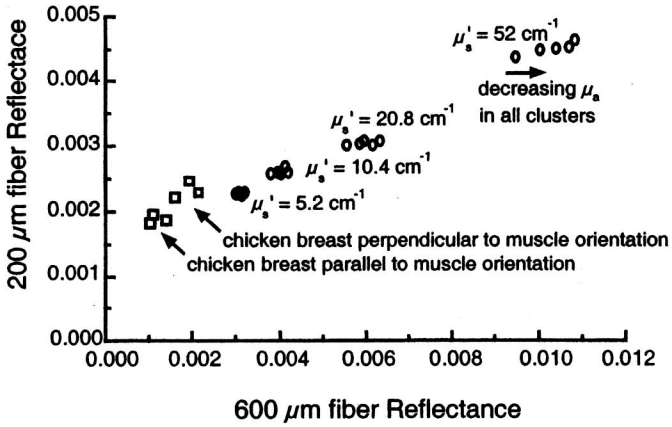

Fig. 4. Measurements of the 20 Intralipid mixtures and repeated measurements of chicken muscle with two distinct fiber orientations relative to the muscle grain. Each cluster is a constant Intralipid concentration with five different absorption coefficients which decrease from left to right.

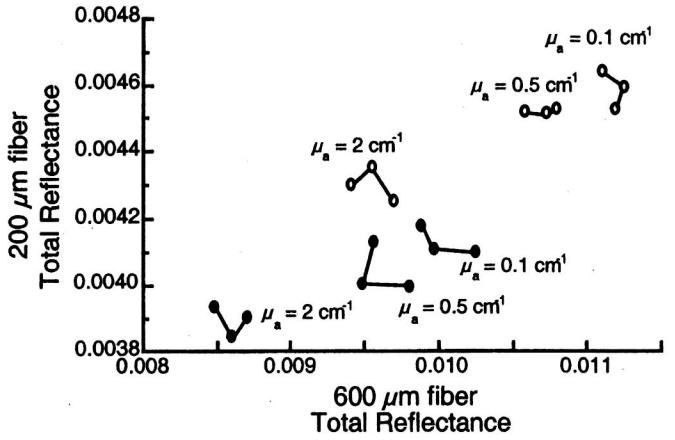

Fig. 5. Independence of sized-fiber measurements for two scattering samples with three different absorption coefficients. Filled circles: $\mu_s' = 47$. Unfilled circles: 52 cm^{-1}. Each joined cluster of three points represents three measurements on a single sample.

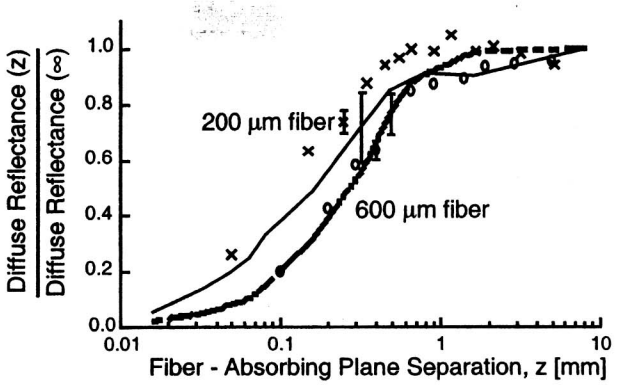

Fig. 6. Signal attenuation for 200- and 600-μm fibers is shown as the fibers approach an absorbing plane of India ink in acrylamide gelatin. The signal is normalized to the diffuse reflectance measured in the intralipid solution far from boundaries ($\mu_s' = 10.4$ cm^{-1}, $\mu_a = 0.5$ cm^{-1}, $g = 0.83$). The curves represent Monte Carlo simulations of the experiment with standard errors of the mean and the points are the experimental data.

In the depth-profiling absorbing plane simulations, 400 000 photons were launched. A perfect absorbing planar boundary was added parallel to the x–y plane. The collected diffuse reflectance was related to the fiber–plane separation distance, simulating the experiment in Section II-D. Additional simulations were performed with the absorption held fixed at 0.5 cm^{-1} while the scattering was varied ($\mu_s' = 8.5$–34 cm^1) and the reduced scattering fixed at 21 cm^{-1}, while absorption was varied ($\mu_a = 0.05$–2.0 cm^1). In the Monte Carlo code, the photon weight became zero when it crossed into the absorbing plane. The location of the boundary, determined by a z position was varied for each set of optical properties.

Finally, the maximum angles for launching and collection were varied independently. The maximum angle (measured from the normal of the fiber face) for the launching photons was varied independent of the collection angle, to simulate under-filling of fiber modes. The maximum launch angle was stepped in 2° increments while the collection angle was held fixed at 12° for the fiber in air. Next, the maximum launch angle was held fixed while the maximum acceptance angle of the fiber was varied to evaluate the sensitivity with respect to numerical aperture. The acceptance angles chosen were concentrated around 13° for the fiber in air (for a NA $\approx$ 0.2) and then extended to include very small and large NA fibers (0.02–0.65). For all simulations the optical properties were held constant with $\mu_s = 61.18$ cm^1, $\mu_a = 0.5$ cm^1, and $g = 0.83$.

III. Results

A. Tissue Model

Fig. 3 shows measurements of the Intralipid array, as well as the results of the Monte Carlo simulations. The experimental variation in measurement was smaller than that returned by the simulations. Typical experimental variation are shown in Fig. 5.

Fig. 4 also shows 20 measurements of the samples (the 4.5% Intralipid are omitted for clarity) along with *in vitro* chicken breast. All concentrations of ink are shown at each Intralipid concentration. Each cluster represents solutions with the same scattering coefficient. Within each cluster, the higher absorbing solution has a lower reflection with respect to the 600-μm fiber reflectance. Marijnissen *et al.* [30] reported a scattering coefficient for chicken muscle ($\mu_s' = 3.3$ cm^1 and $\mu_a = 0.17$ cm^1), which agrees with the data presented here, but the absorption coefficient of chicken is unresolvable with the sized-fiber device for such a low scattering coefficient. Fig. 5 shows a comparison of the 5% Intralipid samples with absorption coefficients of 0.1, 0.5, and 2.0 cm^{-1} with 4.5% Intralipid solutions with the same absorption coefficients. A slight decrease of scattering ($\Delta\mu_s' = 5.2$ cm^1) in one sample relative to another is distinguishable by a drop in the 200 μm fiber reflectance. A drop in the reflectance also occurs as the absorption increases but the effect is more pronounced with the 600-μm fiber reflectance measurement.

B. Monte Carlo Simulations

The effect of attenuation near an absorbing plane is shown experimentally in Fig. 6. Monte Carlo simulations are also shown, which are confirmed by the experimental results. All reflectances are normalized by dividing the perturbed signal by the reflectance that would be measured in the same turbid medium when the fibers are far from any boundaries. Fig. 7

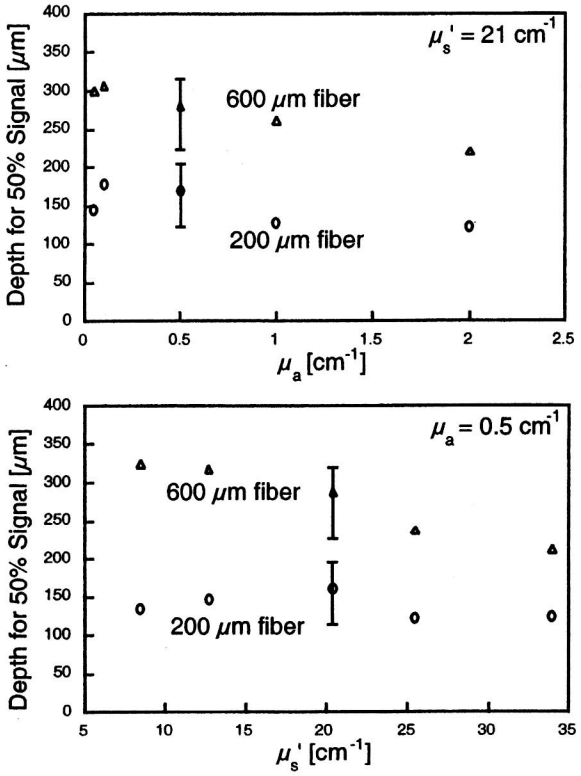

Fig. 7. Monte Carlo simulations show the separation between a fiber and an absorbing plane where a 50% drop in signal occurs for variations in the absorption and scattering properties. The anisotropy is set to 0.83 to simulate Intralipid.

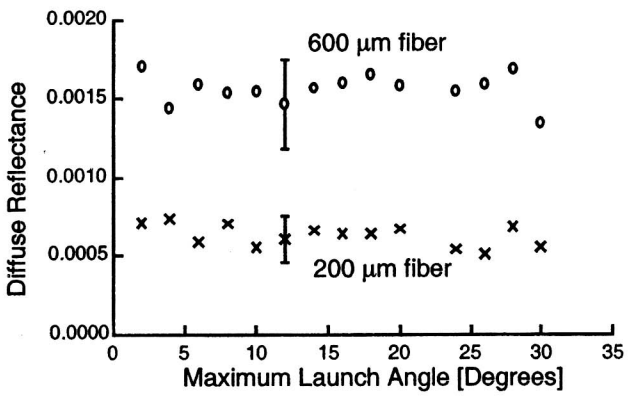

Fig. 8. For a fixed acceptance angle of the fiber, the maximum angle of launch from a Gaussian distribution does not influence the diffuse reflectance collected. This suggests that complete mode filling of the fibers is unnecessary to obtain a consistent result, and by extension, modal variation of the emission does not have any effect upon the measurement. The optical properties used are $\mu_s' = 10.4\ \text{cm}^{-1}$, $\mu_a = 0.5\ \text{cm}^{-1}$, and $g = 0.83$.

shows Monte Carlo results of the 200- and 600-μm fibers, indicating the distance at which the diffuse reflection drops in half due to a perfectly absorbing plane with respect to independent variation of the absorption and scattering properties.

Monte Carlo simulations also show that the photon launch angle has no effect upon the reflectance collected by the fiber as shown in Fig. 8. Thus, the photon launching distribution is inconsequential to the amount of backscattered light collected by the fiber.

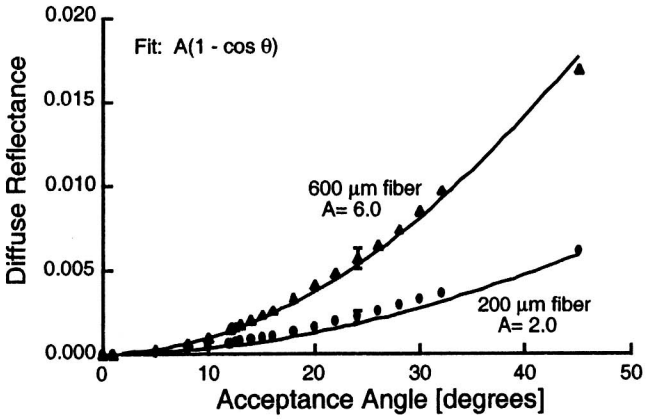

Fig. 9. Fraction of diffuse light collected by each fiber is dependent on the acceptance angle of the fiber θ in air, increasing with a $1 - \cos\theta$ dependence, which follows from a geometrical result if light returns to the fibers uniformly from all directions. A is a scaling parameter to fit the relation. The photon launch angle distribution is held constant and only the acceptance angle of the fiber is varied. The optical properties used are $\mu_s' = 10.4\ \text{cm}^{-1}$, $\mu_a = 0.5\ \text{cm}^{-1}$, and $g = 0.83$.

On the other hand, the numerical aperture of the fiber affects the amount of light collected from the tissue. Fig. 9 shows Monte Carlo simulations which demonstrate how the collected diffuse reflectance varies with the maximum acceptance angle dictated by the fiber numerical aperture. The change in maximum half-angle of acceptance has a $1 - \cos\theta$ relation to the amount of light collected where θ is the half-angle of the maximum cone of light propagated by the fiber.

IV. Discussion

Monte Carlo simulations give information about the photons backscattered into the illumination fiber; in particular, the fraction of light collected by the fiber increases with the maximum angle of acceptance for the fiber following $1 - \cos\theta$. The $1 - \cos\theta$ dependence is the expected geometric result if the light returning to the fiber is uniform in all directions at the fiber face. The fraction of light collected for this case is the ratio of the area of a spherical cap bounded by the numerical aperture cone, divided by the area of a hemisphere $2\pi r^2(1 - \cos\theta)/2\pi r^2 = (1 - \cos\theta)$. Furthermore, the angular distribution for which photons are emitted from the fiber is independent of the fraction of light collected by the fibers as shown in Fig. 8. This is a significant detail which indicates that complete mode filling of a fiber is unnecessary to obtain consistent results, and implies that modal variation in emission does not have any effect upon the measurement. Finally, the angular dependence of both the emission and the collection of photons indicate that light returning to the fiber is uniformly distributed over all directions.

Smaller fibers collect less light and are less sensitive to optical property changes. The relationship between fiber size and sensitivity can be explained by crudely approximating the light returning to the fiber by an isotropic point source, positioned one reduced mean-free path from the fiber face. If $\rho_{\text{fiber}} = (\mu_a + \mu_s')R_{\text{fiber}}$ is the radius of the fiber in reduced mean-free paths, then the half-angle of the cone formed by the point source and the face of the fiber is $\theta_c = \tan^{-1}\rho_{\text{fiber}}$. The fraction of light returning to the fiber can be estimated by the solid angle

subtended the face of the fiber relative to the point source divided by 4π steradians (all directions). This fraction reduces to the form

$$\frac{2\pi \mathrm{mfp}'^2(1-\cos\theta_c)}{4\pi \mathrm{mfp}'^2} = \frac{1}{2}\left(1 - \frac{1}{\sqrt{\rho_{\mathrm{fiber}}^2+1}}\right) \approx \frac{\rho_{\mathrm{fiber}}}{4}$$

where $\mathrm{mfp}' = (1/\mu_a + \mu_s')$ is the reduced mean-free path. For this crude approximation, when $\rho_{\mathrm{fiber}}/4$ drops below 1/12, our system cannot resolve absorption changes less than 2 cm^{-1}. A diffuse point source [16] cannot be used to estimate the amount of the returning light to the fiber because the diffusion approximation is invalid at this distance. In general, as the reduced mean-free path increases, the signal collected decreases such that, for reduced mean-free paths greater than 500 μm, the 200–μm fiber can no longer resolve changes in absorption smaller than a factor of two (e.g., absorption coefficients of 0.5 and 2.0 cm^{-1} are clearly distinct from 1.0 cm^{-1}). The 600-μm fiber can resolve changes in absorption by a factor of two for reduced mean-free paths up to 1900 μm.

We found that the 200- and 600-μm fiber system gives optimal resolution when the reduced scattering coefficient is in the range 20–52 cm^{-1}, corresponding to a reduced mean-free path range of 190–500 μm. In this range, absorption coefficients of 0.1, 0.2, 0.5, 1.0, and 2.0 cm^{-1} are distinct and changes of 5 cm^{-1} in the reduced scattering coefficient are resolved by this system. Tissues within this range at visible wavelengths include but are not limited to aorta, brain, liver, lung, and skin [31]. Differentiation and characterization of tissue is ideally suited for UV/visible wavelengths rather than NIR/IR due to shorter scattering pathlengths in the UV/visible range. When the reduced mean-free path for scattering is 500–1900 μm, only absorption coefficients of 0.1, 0.5, and 2.0 cm^{-1} are distinct. For reduced-scattering mean-free paths above 1900 μm, the absorption coefficient resolution becomes larger than 2 cm^{-1}.

Additionally, we determined that larger fibers collect light from deeper in tissue than smaller fibers. Fig. 6 shows that more than half the signal is from photons traveling 1.2 mean-free paths into the medium for a 200-μm fiber and 1.9 mean-free paths for a 600–μm fiber. The depth for which half of returning photons travel is fairly insensitive to changes in the absorption and the scattering coefficient as shown in Fig. 7. Pogue and Burke [32] suggest that light being collected by a 200-μm fiber has an average of 1.2 scattering events, while the 600-μm fiber has 1.5 scattering events for $\mu_s' = 10$ cm^{-1} and $\mu_a = 0.1$ cm^{-1}, which agrees well with our results, though our results are for an absorption coefficient of 0.5 cm^{-1}. Fig. 7 shows that the mean depth of photon travel does not change significantly for absorption in the range of 0.05–2.0 cm^{-1}. Also, nearly 90% of all the collected photons travel less than 800 μm (approximately one reduced mean-free path) into the medium for both fiber sizes. Effectively, both fibers are sampling the same depth of tissue; however, a greater fraction of photons undergo a single scattering event before returning to the 200-μm fiber than for the 600-μm fiber. In other words, larger fiber diameters collect a greater proportion of multiply scattered photons than smaller fibers.

This study demonstrates feasibility of a sized-fiber device using 200- and 600-μm fibers. We have shown that measurements taken with this device on a Intralipid tissue model agree with our Monte Carlo simulations over a range of absorption 0.1–2.0 cm^{-1}, and reduced scattering 5.2–52 cm^{-1}. However, further studies are needed. An inversion technique relating optical properties to fiber reflectance has yet to be implemented. An empirical relation between reflectance and optical properties would be preferable, yet the 200-μm fiber signal is nearly independent of the absorption properties in the range of this study and may be directly related to the reduced scattering coefficient. The 600-μm signal could then be corrected for scattering to extract the absorption coefficient. With an inversion technique, an *in vivo* study measuring optical properties with the sized-fiber device can be performed. Furthermore, studies on anisotropy need to be addressed to determine if the system can resolve tissues with the same reduced scattering coefficient but differ in anisotropy and scattering coefficients.

Sized-fiber measurements have several advantages. The device is compact and measurements can be taken through a needle or endoscope. Real-time monitoring can be performed with the device using a broad spectral source which is best suited in the UV/visible. System calibration only requires measurement of the Fresnel reflectance of air and water. Finally, the device acquires localized information from a volume less than a cubic millimeter extending no more than a millimeter from the fiber face when absorption is resolved.

ACKNOWLEDGMENT

The authors thank S. Jacques, J. Ramella-Roman, and P. Bargo for their support and insightful discourse.

REFERENCES

[1] B. C. Wilson and M. S. Patterson, "The physics of photodynamic therapy," *Phys. Med. Biol.*, vol. 26, pp. 327–360, 1986.

[2] B. J. Tromberg, L. O. Svaasand, M. K. Fehr, S. J. Madsen, P. Wyss, B. Sasone, and Y. Tadir, "A mathematical model for light dosimetry in photodynamic destruction of human endometrium," *Phys. Med. Biol.*, vol. 41, pp. 233–237, 1996.

[3] M. S. Patterson, B. C. Wilson, J. W. Feather, D. M. Burns, and W. Pushka, "The measurement of dihematoporphyrin ether concentration in tissue by reflectance spectrophotometry," *Photochem. Photobiol.*, vol. 46, pp. 337–343, 1987.

[4] M. A. O'Leary, D. A. Boas, B. Chance, and A. G. Yodh, "Reradiation and imaging of diffuse photon density waves using fluorescent inhomogeneities," *J. Lumin.*, vol. 60–61, pp. 281–286, 1994.

[5] F. F. Jobsis, J. H. Keizer, J. C. LaManna, and M. Rosenthal, "Reflectance spectroscopy of cytochrome aa3 *in vivo*," *J. Appl. Physiol.*, vol. 43, pp. 858–872, 1977.

[6] B. Chance, S. Nioka, J. Kent, K. McCully, M. Fountain, R. Greenfeld, and G. Holtom, "Time resolved spectroscopy of hemoglobin and myoglobin in resting and ischemic muscle," *Anal. Biochem.*, vol. 174, pp. 698–707, 1988.

[7] M. Cope and D. T. Delpy, "System for long-term measurement of cerebral blood and tissue oxygenation on newborn infants by near infrared transillumination," *Med. Biol. Eng. Comput.*, vol. 26, pp. 289–294, 1988.

[8] J. B. Fishkin, O. Coquoz, E. R. Anderson, M. Brenner, and B. J. Tromberg, "Frequency-domain photon migration measurements of normal and malignant tissue optical properties in a human subject," *Appl. Opt.*, vol. 36, pp. 10–20, 1997.

[9] B. J. Tromberg, O. Coquoz, J. B. Fishkin, T. Pham, E. R. Anderson, J. Butler, M. Cahn, J. D. Gross, V. Venugopalan, and D. Pham, "Noninvasive measurements of breast tissue optical properties using frequency-domain photon migration," *Philos. Trans. Roy. Soc. London Ser.*, vol. B 352, pp. 661–668, 1997.

[10] A. Kienle, L. Lilge, M. S. Patterson, R. Hibst, R. Steiner, and B. C. Wilson, "Spatially resolved absolute diffuse reflectance measurements for noninvasive determination of the optical scattering and absorption coefficients of biological tissue," *Appl. Opt.*, vol. 35, pp. 2304–2314, 1996.

[11] J. R. Mourant, I. J. Bigio, D. A. Jack, T. M. Johnson, and H. D. Miller, "Measuring absorption coefficients in small volumes of highly scattering media: Source–detector separations that do not depend on scattering properties," *Appl. Opt.*, vol. 36, pp. 5655–5661, 1997.

[12] M. G. Nichols, E. L. Hull, and T. H. Foster, "Design and testing of a white-light, steady-state diffuse reflectance spectrometer for determination of optical properties in highly scattering systems," *Appl. Opt.*, vol. 36, pp. 93–104, 1997.

[13] M. S. Patterson, B. Chance, and B. C. Wilson, "Time resolved reflectance and transmittance for the noninvasive measurement of tissue optical properties," *Appl. Opt.*, vol. 28, pp. 2331–2336, 1989.

[14] B. W. Pogue and M. S. Patterson, "Frequency-domain optical absorption spectroscopy of finite tissue volumes using diffusion theory," *Phys. Med. Biol.*, vol. 39, pp. 1157–1180, 1994.

[15] R. Cubeddu, A. Pifferi, P. Torricelli, and G. Valentini, "Experimental test of theoretical models for time-resolved reflectance," *Med. Phys.*, vol. 23, pp. 1625–1633, 1996.

[16] T. J. Farrell, M. S. Patterson, and B. Wilson, "A diffusion theory model of spatially resolved, steady-state reflectance for the noninvasive determination of tissue optical properties *in vivo*," *Med. Phys.*, vol. 19, pp. 879–888, 1992.

[17] W. M. Star, "Diffusion theory of light transport," in *Optical-Thermal Response of Laser Irradiated Tissue*, A. J. Welch and M. J. C. van Gemert, Eds. New York: Plenum, 1995, ch. 6, pp. 101–129.

[18] S. L. Jacques and L. Wang, "Monte Carlo modeling of light transport in tissue," in *Optical-Thermal Response of Laser Irradiated Tissue*, A. J. Welch and M. J. C. van Gemert, Eds. New York: Plenum, 1995, ch. 4, pp. 101–129.

[19] T. J. Farrell, B. Wilson, and M. S. Patterson, "The use of neural network to determine tissue optical properties from spatially resolved diffuse reflectance measurements," *Phys. Med. Biol.*, vol. 37, pp. 2281–2286, 1992.

[20] J. S. Dam, T. Dalgaard, P. E. Fabricius, and S. Andersson-Engels, "Multiple polynomial regression method for determination of biomedical optical properties from integrating sphere measurements," *Appl. Opt.*, vol. 39, pp. 1202–1209, 2000.

[21] G. H. Weiss, R. Nossal, and F. Bonner, "Statistics of penetration depth of photons re-emitted from irradiated tissue," *J. Mod. Opt.*, vol. 36, pp. 349–359, 1989.

[22] M. S. Patterson, S. Anderson-Engels, B. C. Wilson, and E. K. Osei, "Absorption spectroscopy in tissue-simulating materials: A theoretical and experimental study of photon paths," *Appl. Opt.*, vol. 34, pp. 22–30, 1995.

[23] F. Bevilacqua, D. Piquet, P. Marquet, J. D. Gross, B. J. Tromberg, and C. Despeursinge, "*In vivo* local determination of tissue optical properties: Applications to the human brain," *Appl. Opt.*, vol. 38, pp. 4939–4950, 1999.

[24] S. A. Prahl and S. L. Jacques, "Sized-fiber spectroscopy," in *SPIE Proc. Laser Tissue Interaction IX*, vol. 3254, S. L. Jacques, Ed., 1998, pp. 348–352.

[25] T. P. Moffitt and S. A. Prahl, "In vivo sized-fiber spectroscopy," in *SPIE Proc. Optical Biopsy III*, vol. 3917, R. R. Alfano, Ed., 2000, pp. 225–231.

[26] S. T. Flock, S. L. Jacques, B. C. Wilson, W. M. Star, and M. J. C. van Gemert, "Optical properties of intralipid: A phantom medium for light propagation studies," *Lasers Surg. Med.*, vol. 12, pp. 510–519, 1992.

[27] J. W. Pickering, S. A. Prahl, N. van Wieringen, J. F. Beek, H. J. C. M. Sterenborg, and M. J. C. van Gemert, "Double-integrating-sphere system for measuring the optical properties of tissue," *Appl. Opt.*, vol. 32, pp. 399–410, 1993.

[28] S. A. Prahl, M. J. C. van Gemert, and A. J. Welch, "Determining the optical properties of turbid media by using the adding-doubling method," *Appl. Opt.*, vol. 32, pp. 559–568, 1993.

[29] H. J. van Staveren, C. J. M. Moes, J. van Marle, S. A. Prahl, and M. J. C. van Gemert, "Light scattering in intralipid-10% in the wavelength range of 400–1100 nm," *Appl. Opt.*, vol. 31, pp. 4507–4514, 1991.

[30] J. P. A. Marijnissen, W. M. Star, J. L. van Delft, and N. A. P. Franken, "Light intensity measurements in optical phantoms and *in vivo* during HpD photoradiation treatment using a miniature light detector with isotropic response," in *Photodynamic Therapy of Tumors and other Diseases*, G. Jori and C. Perria, Eds. Padova, Italy: Libreria Progetto, 1985, pp. 387–390.

[31] W. F. Cheong, S. A. Prahl, and A. J. Welch, "A review of the optical properties of biological tissues," *IEEE J. Quantum Electron.*, vol. 26, pp. 2166–2185, 1990.

[32] B. W. Pogue and G. Burke, "Fiber-optic bundle design for quantitative fluorescence measurement from tissue," *Appl. Opt.*, vol. 37, pp. 7429–7436, 1998.

Theodore P. Moffitt received the B.S. degree in physics (with an optics concentration) from Western Washington University, Bellingham, in 1997, and the M.S. degree in electrical and computer engineering from the Oregon Graduate Institute, Beaverton, in 2000, where he is currently working toward the Ph.D. degree in electrical engineering.

S. A. Prahl, photograph and biography not available at the time of publication.